Non-contact sensing for anomaly detection in wind turbine blades: A focus-SVDD with complex-valued auto-encoder approach

Gaëtan Frusque [a],*, Daniel Mitchell [b], Jamie Blanche [b], David Flynn [b], Olga Fink [a],*

[a] Laboratory of Intelligent Maintenance and Operations Systems, EPFL, Lausanne, Switzerland
[b] James Watt School of Engineering, Autonomous Systems and Connectivity Division, University of Glasgow, University Avenue, Glasgow, G12 8QQ, UK

ARTICLE INFO

ABSTRACT

The occurrence of manufacturing defects in wind turbine blade (WTB) production can result in significant increases in operation and maintenance costs of WTBs, reduce capacity factors of wind farms, and occasionally lead to severe and disastrous consequences. Therefore, inspection during the manufacturing process is crucial to ensure consistent fabrication of composite materials. Non-contact sensing techniques, such as Frequency Modulated Continuous Wave (FMCW) radar, are becoming increasingly popular as they offer a full view – cross sectional analysis – of these complex structures during assembly and curing. In this paper, we enhance the quality assurance of WTB manufacturing utilising FMCW radar as a non-destructive sensing modality. Additionally, a novel anomaly detection pipeline is developed that offers the following advantages: (1) We use the analytic representation of the Intermediate Frequency signal of the FMCW radar as a feature to disentangle material-specific and round-trip delay information from the received wave. (2) We propose a novel anomaly detection methodology called focus Support Vector Data Description (focus-SVDD). This methodology involves defining the limit boundaries of the dataset after removing healthy data features, thereby focusing on the attributes of anomalies. (3) The proposed method employs a complex-valued autoencoder to remove healthy features and we introduces a new activation function called Exponential Amplitude Decay (EAD). EAD takes advantage of the Rayleigh distribution, which characterises an instantaneous amplitude signal. The effectiveness of the proposed method is demonstrated through its application to collected data, where it shows superior performance compared to other state-of-the-art unsupervised anomaly detection methods. This method is expected to make a significant contribution not only to structural health monitoring but also to the field of deep complex-valued data processing and SVDD application. The code and dataset will be made publicly available. The code and dataset are available here [1]

1. Introduction

The wind turbine industry is experiencing consistent expansion within its sector, with projections indicating a compound annual growth rate of 10.1% from 2022 to 2027. As a result of this growth, the wind turbine industry is expected to increase its market size from $18.75 billion in 2020 to $26.82 billion by 2027 [1]. The growth of the wind turbine industry is largely attributed to

advancements in turbine design, such as the use of larger wind turbines, longer turbine blades (measuring over 100 m in length) and the implementation of floating wind turbines, allowing for positioning further from the shoreline [2]. The increasing size and complexity of wind turbine designs have resulted in a greater need for improvements in quality assurance due to the increased risks and complexity when creating larger designs, especially since manufacturing defects can lead to crack formation, propagation under cyclic stresses and defects further in the operational lifecycle [3–5].

Despite wind turbine blade composites manufacturing being predominantly a manual process, efforts have been made to improve the manufacturing method. Automation is an approach which aims at reducing manufacturing cycle duration's alongside consequent manufacturing unit cost reductions [6]. Improvements in manufacturing techniques to date have mainly consisted of developing automation in the layup technique, positioning of blade composite to be prepared for sanding, trimming and grinding, as well as reducing the number of personnel working at height, particularly for larger blades [7]. To improve the accuracy in automation, digital twins are being explored as means to couple real-world data into simulations that improve design and assembly processes, and allow for an overview of quality assurance in the manufacturing phase [8,9]. The intention being that by leveraging historical results and data from SCADA and structural health monitoring techniques to inform current manufacturing at pace that reduces defects occurring in the manufacturing stages [10,11].

Inspection during the manufacturing process is essential to ensure that composite materials are fabricated consistently. It can minimise the occurrence of imperfections, which in turn could lead to complications, resulting in cost overruns and asset downtime. The manufacturing process of composite materials poses several challenges, which can vary depending on the technique used. Consistent hardening of the of composite materials when injecting epoxy resin can be challenging and may result imperfections. Hence, there is a need for sensing methodologies that can verify the quality of the asset as a high quality material. In this research, we employed a non-contact method using Frequency Modulated Continuous Wave (FMCW) radar to inspect defects in epoxy resin injection, which are known to pose challenges. The sensor is low power, lightweight and operates in the K-band. Initial experiments were conducted on replicated defects during Operation and Maintenance (O&M) [12]. This work specifically focuses on quality assurance during the production of composite wind turbine blades.

There are several methods of inspection which are currently available or in development for structural health monitoring within composites. Montazerian et al. conducted a comprehensive review of the various types of sensors that can be embedded within composite materials, including piezoelectric, piezoresistive and optical fiber sensors [13]. However, embedding sensors within a composite being cured can alter the curing process, resulting in delaminations. Hassani et al. present a comprehensive review of structural health monitoring techniques for composite structures detailing the types of damage that can be present on a composite structure via non-destructive testing techniques and vibration-based damage detection [14]. Listed below are some of the critical requirements for sensing methods that emerged as key limitations in the reviewed papers: affordability, continuous monitoring capability, sensitivity to low level of damage, ability to detect different damage types, robustness to different ambient loading conditions, resistance to measured noise, and resilience to environmental factors like weather. Gupta et al. provide an in depth review of sensing technologies for non-destructive evaluation of structural composite materials [5]. The review paper highlights different sensing mechanisms alongside their working principles, setups, advantages, limitations and usage levels for structural composites. The article also provides an insight into current and future research trends for composites and prognostics and health management (PHM). The current research imperative displays a trend towards non-contact sensing, including methods such as digital image correlation, infrared tomography and FMCW. To sum up, current research in the field highlights the difficulties associated with detecting subsurface defects that are present in composite materials. Detecting potential defects or weaknesses in turbine blades during the manufacturing process is critical for effective prognostics and health management. As the turbine blades become larger, the risks associated with undetected defects in the early phases also increase. The primary objective of this article is to improve the quality assurance of manufactured blades using FMCW radar as a non-destructive tool. By using this technology, manufacturing centers can increase production to meet demand while ensuring that high-quality products with extended overall lifecycles and capabilities are delivered to the market.

The FMCW radar is a non-destructive sensing method with the ability to address open challenges in composite structure characterisation via surface and subsurface detection of defects. To date, the sensor has been utilised for several defects within porous dielectric materials including delamination, water ingress, embedded materials and subsurface anomalies. The technology has been applied to sandstones representing civil infrastructure, sandwich and monolithic composite wind turbine blades and tarmac with surface salt dispersions [15–19] In addition, the sensor has the ability to detect dynamic load deformations where for a dynamically compressed sandstone, the sensor provided up to 30 s of warning in sandstone [20]. This article introduces novel framework that combines signal processing and deep learning approaches for detecting anomalies during the manufacturing phase. This work demonstrates the significance of employing FMCW radar for non-invasive real-time data capture and monitoring throughout the entire manufacturing process, rather than during the O&M stage, due to the nature of the simulated manufacturing defect. For example, during resin injection, the sensor could be positioned to monitor the flow rate of injection and identify areas which require more resin to assure successful composite bonding; leading to quality assurance. While composite materials have seen an increase in the wind industry, their usage has also increased due to new use cases within aerospace, hydrogen storage tanks, automotive and civil infrastructure, which will also face similar challenges in future to ensure effective manufacture and operational lifecycle [21–23].

The proposed novel framework makes two methodological contributions that leverages the characteristics of the FMCW radar data. We also recognise the potential transferability of the method to the O&M sector for asset integrity inspection via deployed robotics for improved integrity analysis. Firstly, we introduce an unsupervised anomaly detection approach using support vector data description (SVDD) [24]. Our approach represents a specific case of a one-class classifier, where the model is exclusively trained

using samples of healthy data. Although SVDD is not a new technique for anomaly detection, it has been recently applied various studies such as [25] for rolling bearing performance degradation assessment, [26] for detecting faults in gearbox vibrational signals and [27] for structural health monitoring. The reason behind its recent popularity is its efficient learning capabilities and the ease of interpretation of the obtained results. Although there are notable extensions for semi-supervised cases [28], or data that can be mapped to a graph [29], utilising more advanced strategies such as deep models have not demonstrated better results than the standard approach for unsupervised cases [30]. Our study is to streamline the SVDD task by focusing on the residuals between the expected healthy behavior and the observed one, enabling us to focus on anomaly attributes that deviate from the healthy distribution. To achieve this, we propose a new approach called focus-SVDD that removes healthy data features from the dataset. We propose utilising an Autoencoder (AE) to eliminate these features, and also modify the SVDD boundary to address any potential overfitting issues that may arise from using this model.

Our second methodological contribution involves exploring various representations of the Intermediate Frequency signal, with a focus on the analytical representation. This representation provides a better separation between the effects of round trip propagation and the frequency-dependent reflectivity of the surface target. However, since the analytical signal is complex-valued, an AE capable of handling this type of data is necessary. The use of complex-valued network [31] is a recent development in this field, with applications in remaining useful life prediction of rotating machinery [32], object discovery [33] and speech enhancement [34] . One major challenge faced in this domain is the lack of a standard activation function, such as the Rectified Linear Units (ReLU), used for real-valued autoencoders. In this work, we introduce a novel complex activation function called Exponential Amplitude Decay (EAD) that leverages the Rayleigh distribution of the complex amplitude distribution to achieve better performance.

2. Materials and methods

2.1. Investigation procedure: Monolithic composite

The material under test included a monolithic composite material representing a sample of a wind turbine blade and can be viewed in Fig. 1A with detailed schematic in Fig. 1B. The thickness of the material measured 51.4 mm ± 0.4 at 18 points across the material. The material exhibited a dry adhesive defect typically found during the manufacturing process and is formed during the resin infusion process. This occurs when insufficient resin penetrates the fiberglass material resulting in an uncured adhesive. The regions of uncured adhesive measured approx. 12 cm in height and 10 cm in width. The sample was intentionally created to exhibit this defect using the methods and materials used to construct very large WT blades for offshore use. As seen in Fig. 1B, the red line represents the extent of absent resin on the surface of the sample. The yellow line represents an estimate of where the resin is absent within the sample.

Fig. 1C depicts the FMCW radar setup comprising the electronics that generate the electromagnetic wave and the horn antenna that is attached to it. The controller board requires a 12 V supply and contains a serial port for data extraction. The sensor weighs approximately 400 grams, consumes low power and can detect surface and subsurface defects within dielectric materials and composites. The radar operated from 24–25.5 GHz, bandwidth of 1500MHz with chirp duration of 300 ms and sample rate of 0.2 Hz. To ensure an accurate data collection process, we employed a universal robotic manipulator to automate the process (Fig. 2.). The time taken to complete one scan of the sample was approximately 10 min, where several waypoints were positioned in advance of the scan to cover the full area of the composite. Expecting a recording distance of approximately 10 cm from the surface interface, we acknowledge that slight variations may occur during blade production. To ensure robustness in the face of such operating conditions, we have captured the dataset at three distinct distance ranges: 5 cm, 10 cm, and 15 cm from the surface. This approach ensured continuous scanning of different areas of the sample. The dataset utilised during this research was acquired during the experimentation phase of Tang et al. 2023 [18].

2.2. Data representation

The raw data obtained from the radar sensor is in the time domain and consists of 1501 data points. The signal output from the FMCW sensor is the Intermediate Frequency (IF), which is the difference between the emitted signal and the target interaction with the incident wave. According to [35], the IF signal, noted here $\mathbf{x} \in \mathbb{R}^{1501}$, can be modelled as a superposition of N weighted cosine function such as:

$$x(t) = \sum_{n=1}^{N} a_n \cos(w_n t + \phi_n) \tag{1}$$

where N is the number of radar target or reflective elements. For each target, w_n and ϕ_n are proportional to the round trip propagation time, which is the distance between the target and the radar. The factor a_n is the frequency dependant reflectivity and is a function of the target property and frequency sweep range. As a first step, we standardise the IF signal using the average mean and standard deviation of a set of healthy signals.

To disentangle information about the round trip propagation and frequency dependant reflectivity, we propose using the analytic representation of the signals. The analytic representation is based on the Hilbert transform $\mathcal{I}[\bullet]$ [35], is shown in the following equation when applied to the IF signal:

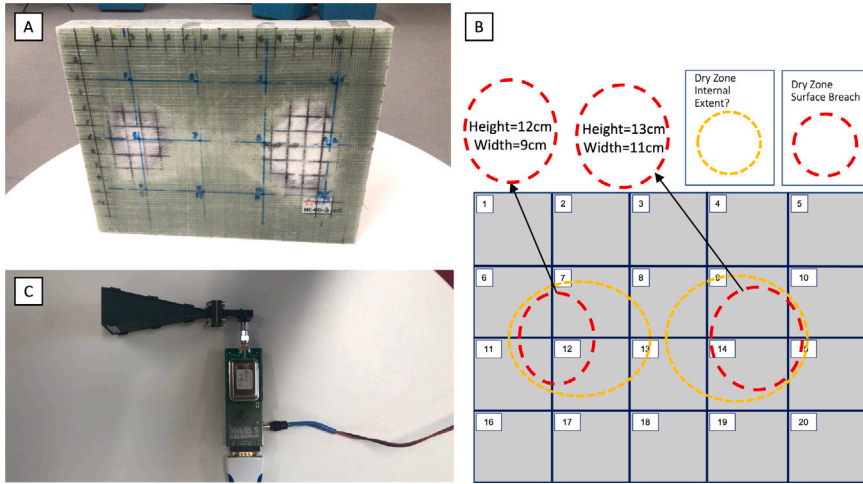$$\mathcal{I}[\mathbf{x}](t) = \sum_{n=1}^{N} a_n \sin(w_n t + \phi_n), \tag{2}$$

Fig. 1. A- Composite with dry adhesive defect, B- Schematic of the monolithic material and C- FMCW radar setup.
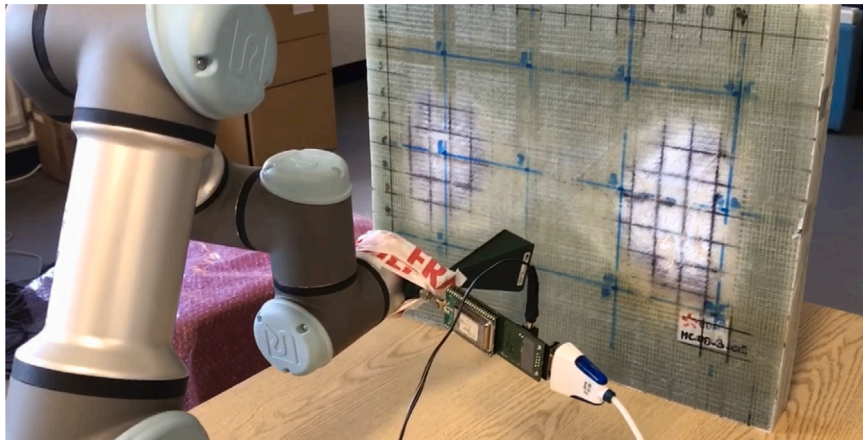

Fig. 2. The data collection technique using FMCW radar and manipulator arm.

The goal of the analytic representation is to propose a natural extension of a real signal in the complex domain by removing the negative frequencies. It can be computed as:

$$\mathbf{x}^{\mathrm{H}} = \mathbf{x} + i\mathcal{I}[\mathbf{x}], \tag{3}$$

Thus by substituting Eqs. (1) and (2) into Eq. (3):

$$x^{\mathrm{H}}(t) = \sum_{n=1}^{N} a_n e^{i(w_n t + \phi_n)}. \tag{4}$$

To ensure an accurate separation of the frequency-dependent reflectivity of the surface and its round-trip propagation time into their respective amplitude and phase, it is essential for the surface of interest to exhibit a higher frequency-dependent reflectivity compared to other reflective elements. This condition necessitates that the radar remains close to the surface of interest. For the radar target with the highest amplitude, which is expected to be the monolithic composite material, we expect its frequency dependant reflectivity amplitude to remain unchanged over time due to the cosine function. Additionally, we anticipate that the round trip propagation time to be encoded in the phase of the signal.

In addition, we propose to study the instantaneous amplitude representation of the IF signal. This will put more emphasis on the frequency dependant reflectivity coefficients. By taking the modulus $|\bullet|$ of the analytic representation, we have:

$$\mathbf{x}^{\mathrm{A}} = |\mathbf{x}^{\mathrm{H}}| \tag{5}$$

Finally, we consider two additional features, that are real-valued representation of complex valued vectors. Considering that $\mathbf{x}^{\mathrm{H}} = |\mathbf{x}^{\mathrm{H}}|e^{i\phi}$, where ϕ is the instantaneous phase of the element of the vector $\mathbf{x}^{\mathrm{H}}$, we consider the feature recently utilised in [36]

and noted $\mathbf{x}^{A\phi}$ which is the concatenation of the instantaneous phase and amplitude of the signals. With $[\mathbf{x}; \mathbf{y}]$ the notation for the concatenation between the two vector $\mathbf{x}$ and $\mathbf{y}$, the feature $\mathbf{x}^{A\phi}$ can be noted as:

$$\mathbf{x}^{A\phi} = \left[|\mathbf{x}^{H}|; \boldsymbol{\phi}\right] \tag{6}$$

Another viable configuration, as employed in previous work, such as in [37], involves concatenating the real and imaginary components. This configuration noted $\mathbf{x}^{RI}$ can be computed as:

$$\mathbf{x}^{RI} = \left[|\mathbf{x}^{H}| \cos(\boldsymbol{\phi}); |\mathbf{x}^{H}| \sin(\boldsymbol{\phi})\right] \tag{7}$$

2.3. Anomaly detection with kernel Support Vector Data Description

Support Vector Data Description (SVDD) is a method developed for dataset characterisation [24]. Its purpose to find the boundary of a dataset and has been successfully used for anomaly detection in various applications [26,27]. Analogous to the support vector machine model, SVDD also uses a kernel function to provide flexibility. The most widely used kernel function is the Radial Basis Function (RBF) [24]. The application of the RBF kernel between two vectors $\mathbf{x}_k$ and $\mathbf{x}_{k'}$ can be written as:

$$\mathcal{K}^{\gamma}(\mathbf{x}_k, \mathbf{x}_{k'}) = e^{-\gamma \|\mathbf{x}_k - \mathbf{x}_{k'}\|_F^2} \tag{8}$$

where $\| \bullet \|_F$ is the Frobenius norm and γ is a free parameter that needs to be carefully choosen. In this work, our focus is solely on the RBF-SVDD method due to its efficiency. The RBF-SVDD can be regarded as a constrained kernel density estimation problem with a density limit $D_{\mathbf{X}_T}^{\gamma}$, which characterises the boundary between healthy and unhealthy samples. This density limit can be expressed as follows:

$$D_{\mathbf{X}_T}^{\gamma} = \sum_{k=1}^{K} \sum_{k'=1}^{K} \alpha_k \alpha_{k'} \mathcal{K}^{\gamma}(\mathbf{x}_k, \mathbf{x}_{k'}) \tag{9}$$

where $\mathbf{X}_T = \{\mathbf{x}_1, \mathbf{x}_2, \ldots, \mathbf{x}_K\}$ is the training dataset containing K healthy samples. Here, $\alpha \in \mathbb{R}^K$ is a vector that describes the importance of each training vector to characterise the density distribution of the dataset. The vector α is computed by minimising the following optimisation problem:

$$\underset{\alpha}{\arg\min} \quad D_{\mathbf{X}_T}^{\gamma} \tag{10}$$
$$\text{s.t.} \quad \sum_{k=1}^{K} \alpha_k = 1,$$
$$0 \leq \alpha_k \leq C \quad \forall k \in \{1, \ldots, K\}.$$

where C is the SVDD hyperparameter that can take values from the segment $[\frac{1}{K}, 1]$. When $C = \frac{1}{K}$, the optimisation problem has a straightforward solution with $\alpha_k = \frac{1}{K} \forall k$ due to its constraints. In this case, all vectors are support vectors, which corresponds to a basic case of kernel density estimation. This approach does not include the data at the border or the outliers in the density limit. In contrast, when $C = 1$, the optimisation problem is less constrained, and the support vectors represent the border of the dataset. All training data are then included in the density limit, and the optimisation problem, shown in Eq. (10) can be solved using linear programming. Considering the optimal values of α for a fixed parameter C and the training dataset $\mathbf{X}_T$, one can compute the value of the density $d_{\mathbf{X}_T}^{\gamma}(\mathbf{x})$ for any sample $\mathbf{x}$ using the following formula:

$$d_{\mathbf{X}_T}^{\gamma}(\mathbf{x}) = \sum_{\mathbf{x}_k \in \mathbf{X}_T} \alpha_k \mathcal{K}^{\gamma}(\mathbf{x}_k, \mathbf{x}) \tag{11}$$

We can use the previously computed density limit $D_{\mathbf{X}_T}^{\gamma}$ to create a decision function $\mathcal{F}^{\gamma}(\mathbf{x})$ that detects if the sample $\mathbf{x}$ is part of the healthy training dataset, labeled as 0, or an abnormal sample, labeled as 1, based on its density value. If the density value of $\mathbf{x}$ is below the density limit, it is considered an abnormal sample, and if it is above, it is considered part of the healthy training dataset. We have:

$$\mathcal{F}^{\gamma}(\mathbf{x}) = \begin{cases} 0 \text{ if } d_{\mathbf{X}_T}^{\gamma}(\mathbf{x}) \geq D_{\mathbf{X}_T}^{\gamma}, \\ 1 \text{ if } d_{\mathbf{X}_T}^{\gamma}(\mathbf{x}) < D_{\mathbf{X}_T}^{\gamma}. \end{cases} \tag{12}$$

2.4. Focus-SVDD for abnormal feature detection

2.4.1. Focus by removing information about the healthy state

While the SVDD aims to find the distribution of the healthy condition from the training dataset, it can be difficult to assess this distribution under different operating conditions of a system. In this work, we propose not to apply the SVDD directly to a raw dataset. Instead, we suggest applying it to a residual dataset where the new samples, denoted as $\mathbf{r}$ can be computed as:

$$\mathbf{r} = \mathbf{x} - \mathcal{H}(\mathbf{x}). \tag{13}$$

Here, $\mathcal{H}(\bullet)$ is a function that computes the best explanation of $\mathbf{x}$ while assuming it is part of the healthy dataset. Thus, $\mathbf{r}$ only contains values that indicates a deviation from the healthy state. We propose to use an autoencoder trained only with healthy data to estimate the function $\mathcal{H}(\bullet)$ and denote the approximation as $H_\theta(\bullet)$ where θ represents the trainable parameters of the autoencoder. To train the autoencoder, we aim to find the values of θ that minimise the error between the input and its reconstruction:

$$\underset{\theta}{\arg\min} \sum_{\mathbf{x}_k \in \mathbf{X}_T} \|\mathbf{x}_k - H_\theta(\mathbf{x}_k)\|_F^2, \tag{14}$$

Notice that autoencoders are widely used for anomaly detection in various fields [38–40]. Similar to the SVDD method, the training of this model also involves using only healthy samples, and the decision is based on the residual norm [41]. However, this approach assumes the residual data follows an isotropic multivariate Gaussian distribution, which may not always hold in practical applications. To address this issue, we suggest estimating a more complex boundary using SVDD instead of using the norm of the residual. Additionally, we anticipate that there will be greater variation in density values when comparing raw data to abnormal sample residuals. It is important to highlight that we opt for SVDD over deepSVDD [42]. The overparametrization in the latter model poses challenges in maintaining a robust boundary, especially considering the size of the data we use for training.

2.4.2. Anomaly detection with focus-SVDD

We denote the residual training dataset $\mathbf{R}_T$ as follows:

$$\mathbf{R}_T = \{\mathbf{x}_1 - H_\theta(\mathbf{x}_1), \mathbf{x}_2 - H_\theta(\mathbf{x}_2), \dots, \mathbf{x}_K - H_\theta(\mathbf{x}_K)\} \tag{15}$$

The RBF-SVDD is applied to the residual data and solves the optimisation problem in Eq. (10) using the density limit $D_{\mathbf{R}_T}^\gamma$. The density limit $D_{\mathbf{R}_T}^\gamma$ is obtained by computing the value of Eq. (9) using the residual training data instead of the raw data. By using the optimal values of α, this leads to a new density function $d_{\mathbf{R}_T}^\gamma(\bullet)$, which is given by Eq. (11) and computed using the residual data. Therefore, the decision function of focus-SVDD is:

$$\mathcal{F}_r^\gamma(\mathbf{x}) = \begin{cases} 0 \text{ if } d_{\mathbf{R}_T}^\gamma(\mathbf{x} - H_\theta(\mathbf{x})) \geq D_{\mathbf{R}_T}^\gamma, \\ 1 \text{ if } d_{\mathbf{R}_T}^\gamma(\mathbf{x} - H_\theta(\mathbf{x})) < D_{\mathbf{R}_T}^\gamma. \end{cases} \tag{16}$$

2.4.3. Density limit correction

A key issue when using autoencoders is the difficulty in assessing how much the network overfits to the training dataset. Furthermore, when applied to a dataset with different operating conditions, the SVDD may lack robustness. In this work, we propose a simple modification of the density limit, denoted D_m^γ, using a validation dataset $\mathbf{X}_V$ containing healthy samples only. We hypothesise that overfitting of the autoencoder, or a new operating condition, may induce a systematic bias in the density values. To correct this bias, we propose the following modification:

$$D_m^\gamma = D_{\mathbf{R}_T}^\gamma - m_T + m_V. \tag{17}$$

where m_T is the mean density value of the training dataset $\mathbf{R}_T$ and m_V is the mean density value of the validation dataset $\mathbf{R}_V$. The modified decision function of the focus-SVDD can be expressed as follows:

$$\mathcal{F}_m^\gamma(\mathbf{x}) = \begin{cases} 0 \text{ if } d_{\mathbf{R}_T}^\gamma(\mathbf{x} - H_\theta(\mathbf{x})) \geq D_m^\gamma, \\ 1 \text{ if } d_{\mathbf{R}_T}^\gamma(\mathbf{x} - H_\theta(\mathbf{x})) < D_m^\gamma. \end{cases} \tag{18}$$

2.5. Proposed activation function for complex-valued AE

2.5.1. Complex-valued AE

In this paper, we propose to use a simple architecture for the autoencoder composed of linear layers and Rectified Linear Units (ReLU) activation functions [43]. Considering a value x, we have $\mathrm{ReLU}(x) = \max(0, x)$. However, since the analytic representation $\mathbf{x}^H$ is a vector of complex values, the ReLU activation function cannot be used in that case. There exist some extensions of the ReLU activation function for complex valued autoencoder [31]. To account for the polar representation of a complex number $z = |z|e^{i\phi_z}$, where ϕ_z denotes the phase value, the most widely used extension of the ReLU layer is [44]:

$$\mathrm{CReLU}(z) = \mathrm{ReLU}(|z|\cos(\phi_z)) + i\mathrm{ReLU}(|z|\sin(\phi_z)). \tag{19}$$

The application of Eq. (19) involves applying the ReLU activation function to the real and imaginary parts of the complex number z. Another common extension involves soft-thresholding the amplitude of the complex number z, which can be written as [45]:

$$\mathrm{modReLU}(z) = \mathrm{ReLU}(|z| - b)e^{i\phi_z}, \tag{20}$$

where b is a trainable parameter. However, this second activation function was shown to perform worse than Eq. (19) in practice [45]. To explain this behavior, we first make the assumption that the output of a complex-valued linear layer node follows
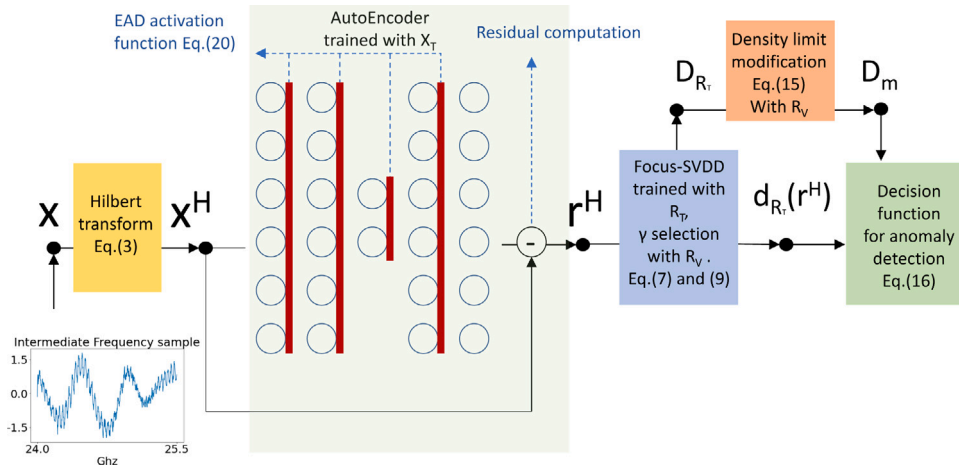
Fig. 3. Proposed framework for anomaly detection using IF signal of FMCW radars, $\mathbf{X}_T$ corresponds to the training dataset, $\mathbf{R}_T$ and $\mathbf{R}_T$ correspond respectively to the residual training and validation dataset.

a centered complex Gaussian distribution. This assumption can be supported by applying the central limit theorem. Thus, we can know the distribution of the modulus $r = |z|$ which follows a Rayleigh distribution with parameter Ω:

$$p(r) = 2\Omega r e^{-\Omega r^2} \tag{21}$$

This distribution has the disadvantage of be skewed and leptokurtic, impeding the learning of the trainable parameter b. Moreover, the threshold is done starting from low values, which are the thin-tailed part of the distribution, outputting a data distribution that is still skewed and leptokurtic. This is a notable difference between the application of the ReLU activation function on real input assumed to be Gaussian or uniform.

2.5.2. Exponential amplitude decay activation function

In this work, we propose a new activation function called Exponential Amplitude Decay (EAD). This new extension of the ReLU layer for complex number is denoted as:

$$EAD(z) = (1 - e^{-b|z|^2})e^{i\phi_z} \tag{22}$$

The proposed EAD activation function has several advantages. Firstly, it is a smooth differentiable function. Secondly, it constrains the amplitude values to remain within the unit circle, which is not the case with the other two activation functions where the output can have arbitrary high values. Finally, when trainable parameter $b = \Omega$, the resulting variable $v = P(r) = 1 - e^{-br^2}$ follows a uniform distribution from 0 to 1. This can be proven by observing that $P(r)$ is the cumulative distribution function of the Rayleigh distribution. Consequently, the amplitudes distribution is non-skewed and thin-tailed, which is not the case for the modReLU activation function.

Finally, one advantage of the EAD activation function is its ability to compute the mean, variance, skewness, and kurtosis statistics of the amplitudes for any value of b. The analytical formulas for these statistics are provided in Appendix, which provides interpretability to the output of each layer of the network.

The proposed approach is summarised in Fig. 3

3. Experiment

3.1. Preprocessing and parameter selection

The dataset was divided into three subsets: the training dataset $\mathbf{X}_T$, the validation dataset $\mathbf{X}_V$, and the test dataset $\mathbf{X}_A$. The training and validation datasets included only samples from the healthy condition, while the test dataset contained both healthy and abnormal samples. A total of 530 healthy samples and 362 abnormal samples were available for testing. For the experiment, a 5-fold cross-validation was proposed. In this setup, 318 healthy samples were used in $\mathbf{X}_T$, 106 healthy samples were used in $\mathbf{X}_V$, and the remaining 106 healthy samples were used in $\mathbf{X}_A$. The abnormal samples were present only in the test dataset $\mathbf{X}_A$.

To determine the optimal γ value for the RBF kernel, we perform a grid search to identify the highest possible value of γ at which a fraction ϵ of the validation dataset is flagged as anomalous. In this study, we have set $C = 1$. There are two main reasons behind this decision. Firstly, opting for $C = 1$ will result in a more detailed boundary for distinguishing between healthy and unhealthy samples. This is a key benefit when employing focus-SVDD compared to relying on the residual norm of the autoencoder. Furthermore, we are in a situation where we are rather confident in the accuracy of the labeling, even though there may be some noise contamination associated with the anomaly. During radar passage through the surface, it may approach nearby areas of damage, leading to reflected

Table 1
Average F1 score over the 5 fold for different signal representation and decision function.

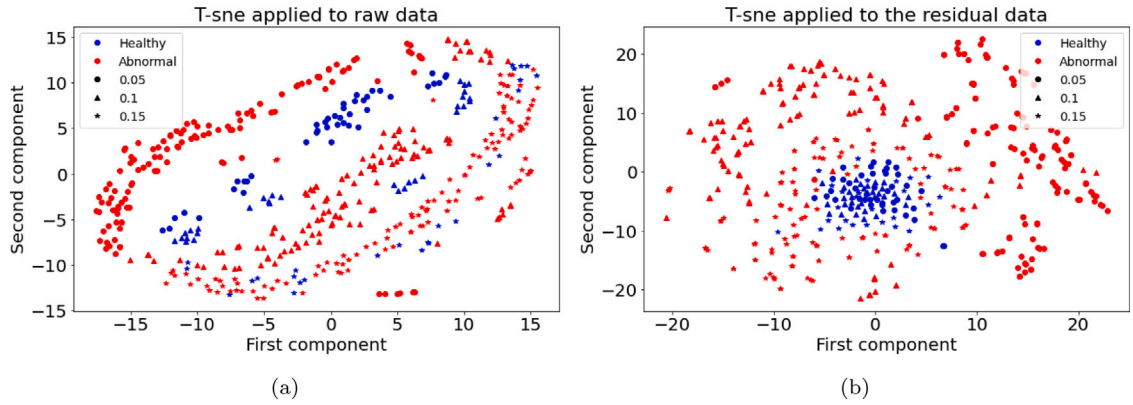|	$\mathcal{F}^\gamma$ (Eq. (12))	$\mathcal{F}^\gamma$ (Eq. (12) with D_m)	$\mathcal{F}_r^\gamma$ (Eq. (16))	$\mathcal{F}_m^\gamma$ (Eq. (18))
$\mathbf{x}$	0.822	0.825	0.884	**0.946**
$\mathbf{x}^A$	0.795	0.795	0.916	**0.920**

Fig. 4. T-SNE representation with a perplexity of 50 of (a) - the IF test data $\mathbf{X}_A$ (b) - the residual data $\mathbf{R}_A$ after training an AE on the IF training dataset. The point shapes correspond to the distance between the radar and the surface, with possible values of 0.05, 0.1, or 0.15 m.

information from the abnormal region and potentially introducing noise that affects healthy data. However, the labeling method we employed offers specificity regarding the locations of anomalies within the dataset. Finally, We have chosen ϵ to be 0.05 since we have observed that it leads also to a more specific decision boundary and yields superior results when using this approach for all methods. Regarding the AE, the encoder network consists of two dense layers of 64 nodes plus one of 32 nodes while the decoder is composed of two dense layers of 64 nodes. We use the ReLU activation function (or one of its complex extensions) in each layer except for the last one.

3.2. Ablation study 1: focus-SVDD

We conducted two ablation studies to evaluate the effectiveness of the one on focus SVDD and the EAD activation function. The first study compares the performance of focus-SVDD methodology to standard SVDD. Table 1 presents the average F1 scores obtained from five folds when using the real signal $\mathbf{x}$ or its instantaneous amplitude $\mathbf{x}^A$ as inputs for three different decision functions: $\mathcal{F}^\gamma$ (Eq. (12)), $\mathcal{F}_r^\gamma$ (Eq. (16)), and $\mathcal{F}_m^\gamma$ (Eq. (18)). To remind, $\mathcal{F}^\gamma$ applies SVDD directly to the raw data, while the other two decision functions are instances of focus-SVDD that use either the density limit $D_{\mathbf{R}_T}$ or the modified density limit D_m. We also present the results of applying the standard decision function (Eq. (12)) with the modified density limit (D_m). The results suggest that the performance is comparable when using the standard SVDD decision function $\mathcal{F}^\gamma$, regardless of whether we use the density limit $D_{\mathbf{X}_T}$ or D_m. This is because the density values of the validation dataset are not expected to differ significantly from those of the training dataset, and thus $D\mathbf{X}_T$ and D_m are similar. However, there is a significant improvement in performance when using the focus-SVDD methodology and the modified density limit, particularly when considering the real signal as input $\mathbf{x}$. This results in an increase in F1 score of 0.062. Morevoer, the focus-SVDD approach outperforms the standard SVDD anomaly detection method by up to an F1 score of 0.121.

In Fig. 4, we used t-Distributed Stochastic Neighbor Embedding (t-SNE) [46] with a perplexity of 50 to analyze the IF test data $\mathbf{X}_A$ and the residual data $\mathbf{R}_A$ obtained after training an AE on the IF training dataset $\mathbf{X}_T$. As one of the most important operating condition we show using different shapes the distance between the radar and the surface, with possible values of 0.05, 0.1, or 0.15 m. Fig. 4 shows that the IF consists of several clusters mostly related to the three operating conditions. Notably, the third operating condition appears to be the most difficult to assess, with an unclear boundary between healthy and unhealthy samples. Identifying the density limit using SVDD may be challenging due to the need for adapting to varying clusters. However, after applying the AE to compute the residual, the dataset was predominantly composed of a single main cluster.We can also see that the samples from the third operating condition are now grouped together.

It is important to highlight that employing a PCA dimensionality reduction method instead of the non-linear t-SNE would result in a much more mixed representation of samples between the healthy and unhealthy conditions in Fig. 4.(b). This indicates that a simple circular boundary, as provided by the autoencoder's residual, is insufficient for effectively distinguishing between healthy and anomalous instances. SVDD becomes a relevant solution to derive a data-driven and refined boundary.

Table 2
Average F1 score over the 5 folds using different activation function and decision function.

	Norm	$\mathcal{F}_r^\gamma$ (Eq. (16))	$\mathcal{F}_m^\gamma$ (Eq. (18))
$\mathbf{x}$	0.916	0.884	**0.946**
$\mathbf{x}^A$	0.841	0.916	**0.920**
$\mathbf{x}^{A\phi}$	0.692	0.872	**0.890**
$\mathbf{x}^{RI}$	0.913	0.885	**0.950**
$\mathbf{x}^H$ (CReLU)	0.931	0.878	**0.941**
$\mathbf{x}^H$ (modReLU)	0.884	**0.905**	0.895
$\mathbf{x}^H$ (EAD)	0.940	0.928	**0.958**

3.3. Ablation study 2: EAD activation function

In order to characterise the EAD activation function and its advantages over other activation functions, we show in Table 2 the average F1 score over five folds for all three signal representations and the three different complex extensions of the ReLU activation function when using the analytic representation $\mathbf{x}^H$. In the 'Norm' case, the decision is based on the residual norm of the autoencoder, where a proportion ϵ of the validation dataset is identified as abnormal. The results show that the autoencoder using the EAD activation function and analytical representation $\mathbf{r}^H$ outperforms all other models when using the 'Norm' method, achieving an F1 score 0.024 higher than the baseline case that uses the signal $\mathbf{x}$ with a real-valued autoencoder. Moreover, it outperforms the state-of-the-art complex-valued activation function CReLU by 0.009. The density limit modification is crucial, as it leads to a significant increase in performance for most cases. Specifically, when using the analytical residual $\mathbf{r}^H$ with CReLU activation function, we observe an improvement of up to 0.064, except for the case of modReLU, which exhibits a drop in performance of 0.01. Generally, using the $\mathcal{F}_r^\gamma$ decision function leads to decreased performance compared to the 'Norm' decision method. However, using the decision function $\mathcal{F}_m^\gamma$ with modified density limit D_m outperforms the other methods and the best F1 score is obtained by combining the $\mathcal{F}_m^\gamma$ decision function with the EAD activation function, achieving a score of 0.958.

In recent work [36,37], there is a prevailing preference for reconfiguring complex inputs to avoid adapting the entire network structure for complex values. To highlight the benefits of the complex-valued neural network, we compare it to the real-valued neural network with as input the real-valued representation of the complex-valued data, composed of the features $\mathbf{x}^{RI}$ and $\mathbf{x}^{A\phi}$. We achieved comparable performance to that of real signals with $\mathbf{x}^{RI}$, likely due to the dataset containing real signals. However, when employing Focus-SVDD with density limit modification, we attained an even higher F1-score, improving it from 0.946 to 0.950. In the case of $\mathbf{x}^{A\phi}$, the results deteriorated compared to real signals, which might be attributed to the neural network struggling to grasp the circular nature of the instantaneous phase data. This feature is a good example of the advantages of using a density limit estimated from the SVDD instead of the norm of the residuals, enhancing the F1-score from 0.692 to 0.872. This can be explained by the fact that phases and amplitudes exist in distinct amplitude ranges, where the hypersphere boundary induced by the norm of the residual is not relevant in this scenario.

In Fig. 5, we demonstrate how the use of our EAD activation function results in the propagation of stable and sub-Gaussian data distribution throughout the network. We display the normalised skewness and excess kurtosis (calculated by subtracting three from the normalised kurtosis) of the amplitude distribution after each layer of the AE for the three activation functions. The green areas represent data distribution with low skewness and platykurtosis which are indicative of a sub-Gaussian distribution. The red dotted lines depict the statistics of the uniform distribution. ModRelu and CReLU both produce heavily skewed and leptokurtic amplitudes, indicating a lack of robustness during training. After applying AED, the resulting distribution is in the green area for both statistics in three out of the five layers. For two layers, the statistics are very close to a uniform distribution. It appears that the proposed activation function is able to improve the network performances by propagating light-tailed amplitude distributions throughout the network.

3.4. Comparison to other unsupervised anomaly detection methods

Finally, we compare the performances of our approach with other state of the art unsupervised anomaly detection method. In Table 3, we compare the focus-SVDD method with EAD activation function to other unsupervised anomaly detection methods, namely K-Nearest Neighbors using (KNN) [47], Isolation Forest (IForest) [48], DeepSVDD [42], Local Outlier Factor (LOF) [49], the AutoEncoder (AE) the Variational AutoEncoder (VAE) [50]. Our implementation of KNN, IForest, DeepSVDD, LOF and VAE are consistent with the APIs of PyOD, which is a comprehensive and scalable Python toolkit for outlier and anomaly detection [51]. All the mentioned methods provide a score. In order to keep consistency with the focus-SVDD, the decision is made based on the score value where a proportion ϵ of the validation dataset are considered as abnormal samples. We employ the parameters that demonstrated effective results on datasets characterised by low levels of noise contamination from abnormal samples [30]. We set the number of neighbors to 5 in KNN and 20 for LOF. We set the number of tree to 100 for the IForest method. Finally, for the DeepSVDD, we use the encoding architecture of the focus-SVDD method with a ℓ_2 regularisation of 0.001 and for the VAE we use exactly the same architecture as the focus-SVDD methodology. For the VAE, the loss function is modified because a second term is added: the Kullback–Leibler Divergence between the unit Gaussian and the latent distribution, however, only the reconstruction error is used for the anomaly score. Since those method are designed for real data, we use the real signal $\mathbf{x}$ as input for comparison.
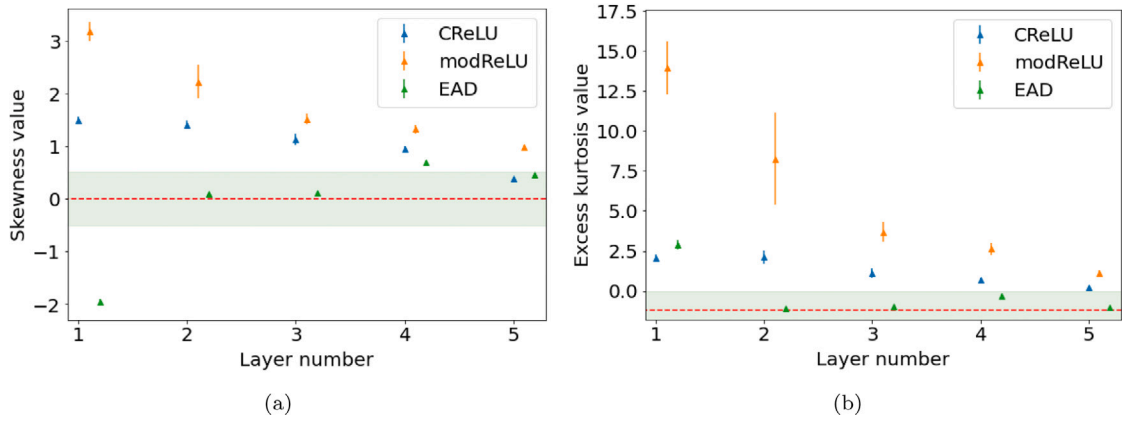
Fig. 5. Mean and standard deviation of (a) Skewness and (b) Kurtosis of the amplitude distribution calculated after each layer of the AE for the three activation functions. In (a) the green area corresponds to low skewness value, in (b) it corresponds to light-tail distribution. The red dotted lines are the statistics of the uniform distribution.

Table 3
Anomaly detection performances of different methods. (Acc.= Accuracy score, Prec.= Precision score).

Method	F1	Acc.	AUC	Prec.	Recall
focus-SVDD	**0.96**	**0.93**	**0.982**	0.94	**0.97**
KNN	0.90	0.85	0.971	0.97	0.83
IForest	0.75	0.69	0.92	0.97	0.62
DeepSVDD	0.81	0.75	0.87	0.97	0.70
LOF	0.90	0.86	0.970	**0.98**	0.84
AE	0.92	0.89	0.970	0.97	0.85
VAE	0.87	0.81	0.95	0.97	0.78

All the previously mentioned methods provide a score. In order to keep consistency with the focus-SVDD, the decision is made based on the score value where a proportion ϵ of the validation dataset are considered as abnormal samples. In summary, the performance of each method is evaluated based on F1 score, accuracy, Area Under the Curve (AUC), precision, and recall. The focus-SVDD method outperforms the other models in terms of F1 score, accuracy, AUC, and recall. In contrast, methods such as KNN and Local Outlier Factor (LOF), which use the boundary of the dataset, have a very good AUC score compared to methods that estimate the distribution of the dataset, such as Variational AutoEncoder (VAE) or DeepSVDD.

4. Conclusion

In this study, we have identified a candidate sensing modality, FMCW radar, for supporting the surface and subsurface analysis of composite – WTB – samples. We utilise a robotic manipulator for the collection of data from the sensing modality. We demonstrate a novel anomaly detection pipeline that utilises FMCW radar as a non-destructive sensing modality as to enhance the quality assurance of WTB manufacturing processes. Using composite material samples, the analytic representation of the IF signal of the FMCW radar is utilised to distinguish between the information related to the round-trip propagation and the frequency dependent reflectivity. We propose a new methodology for anomaly detection, called focus-SVDD, which involves characterising the limit boundaries of the residual dataset by removing healthy data features that are mainly related to the operating conditions and are not relevant for the anomaly detection task. Our approach utilises a complex-valued autoencoder and introduces a novel activation function called EAD, which takes advantage of the Rayleigh distribution to effectively deskew the amplitudes of the output in each layer of the network. To demonstrate the benefits of utilising the SVDD on the residual data rather than directly on the raw data, we conduct an ablation study. We also emphasise the significance of modifying the density limit in this scenario as the autoencoder's behavior is susceptible to overfitting. In addition, we show that our proposed activation function outperforms other complex activation functions and that utilising the analytic representation of the IF signal is more advantageous than using the raw IF signal. Finally, we compare our pipeline with a state-of-the-art unsupervised methodology, and the results show superior performance with an F1 score of 0.96, which surpasses the best performing SOTA method by a margin of 0.04. These findings suggest that our approach holds promise for enhancing the quality assurance of the manufacturing process of WTB and other composite structures.

This work highlights several promising avenues for future research in asset integrity and quality assurance inspections. A trend exists in the robotic deployment of sensors to reduce risks (in both manufacturing and operational phases) and increase accuracy of inspections. A pathway leading to robotic deployment includes testing robotic systems in a controlled environment utilising the non-destructive tool. Additionally, the development of deployment modes and parameter settings optimised for the manufacturing environment, such as gantries above a manufacturing site to facilitate rapid scanning, is essential. To meet this need, the data

acquisition rate will be increased to reduce the time required to perform integrity assessment. This will enable data and results from the FMCW radar to be fed into a centralised database to facilitate optimised decision making for quality assurance or damage identification and rectification. Our proposed focus-SVDD approach has the potential to be extended to a semi-supervised approach, where a semi-supervised deep models estimate the boundary of the healthy class. In conclusion, the suggested approach has the potential for application in other non-destructive detection scenarios. While thermographic and radiographic methods that generate images, and the acoustic methods need adapted autoencoder for the focus-SVDD strategy, the entire framework would be directly applicable to ultrasonic and ground-penetrating radar.

Declaration of competing interest

The authors declare the following financial interests/personal relationships which may be considered as potential competing interests: Frusque reports financial support was provided by Innosuisse Swiss Innovation Agency. Mitchell reports financial support was provided by Offshore Robotics for Certification of Assets.

Data availability

Data will be made available on request.

Acknowledgments

Researchers using this data set should acknowledge the Smart Systems Group University of Glasgow and cite this paper and the following paper within their references which have created this data library of FMCW analysis of composites [18].

Appendix. Statistics of the EAD activation function.

Considering that the output of a complex-valued linear layer follows a Rician distribution with parameter Ω, it is possible to estimate the statistics of the amplitudes after the application of the EAD activation function (Eq. (22)) for any value of the trainable parameter b. The statistics μ, σ, ν, and κ, corresponding respectively to the mean, standard deviation, normalised skewness, and normalised kurtosis of the variable $u = e^{-br^2}$, when r follows a Rician distribution, have an analytical solution, and are as follows:

$$\mu = \mathrm{E}[e^{-br^2}], \tag{A.1}$$

$$= \int_0^\infty e^{-br^2} p(r) dr,$$

$$= 2\Omega \int_0^\infty r e^{-(\Omega+b)r^2} dr,$$

$$= \frac{\Omega}{\Omega + b}.$$

$$\sigma^2 = \mathrm{E}[(e^{-br^2} - \mu)^2], \tag{A.2}$$

$$= \mathrm{E}[e^{-2br^2}] - \mu^2,$$

$$= \frac{\Omega}{\Omega + 2b} - \left(\frac{\Omega}{\Omega + b}\right)^2.$$

$$\nu = \mathrm{E}\left[\left(\frac{e^{-br^2} - \mu}{\sigma}\right)^3\right], \tag{A.3}$$

$$= \frac{1}{\sigma^3}(\mathrm{E}[e^{-3br^2}] - 3\mu\sigma^2 - \mu^3),$$

$$\sigma^3\nu = \frac{\Omega}{\Omega + 3b} - 3\left(\frac{\Omega}{\Omega + b}\right)\left(\frac{\Omega}{\Omega + 2b}\right) + 2\left(\frac{\Omega}{\Omega + b}\right)^3.$$

$$\sigma^4\kappa = \mathrm{E}\left[\left(e^{-br^2} - \mu\right)^4\right], \tag{A.4}$$

$$= \frac{\Omega}{\Omega + 4b} - 4\left(\frac{\Omega}{\Omega + b}\right)\left(\frac{\Omega}{\Omega + 3b}\right) + 6\left(\frac{\Omega}{\Omega + b}\right)^2\left(\frac{\Omega}{\Omega + 2b}\right) - 3\left(\frac{\Omega}{\Omega + b}\right)^4.$$

When $b = \Omega$, we obtain the statistics of an uniform distribution from 0 to 1, i.e. $\mu = \frac{1}{2}$, $\sigma = \frac{1}{12}$, $\nu = 0$ and $\kappa = \frac{9}{5}$ ($-\frac{6}{5}$ considering excess kurtosis).

References

[1] GlobeNewswire, Wind turbine rotor blade market - growth, trends, COVID-19, 2022.

[2] Daniel Mitchell, Jamie Blanche, Sam Harper, Theodore Lim, Ranjeetkumar Gupta, Osama Zaki, Wenshuo Tang, Valentin Robu, Simon Watson, David Flynn, A review: Challenges and opportunities for artificial intelligence and robotics in the offshore wind sector, Energy AI 8 (2022) 100146.

[3] Udayanga Galappaththi, Uik Galappaththi, Am De Silva, Milos Draskovic, M Macdonald, Strategic quality control measures to reduce defects in composite wind turbine blades renewable energy and power quality Journal (RE&PQJ) strategic quality control measures to reduce defects in composite wind turbine blades, 2013.

[4] P.J. Schubel, R.J. Crossley, E.K.G. Boateng, J.R. Hutchinson, Review of structural health and cure monitoring techniques for large wind turbine blades, Renew. Energy 51 (2013) 113–123.

[5] Ranjeetkumar Gupta, Daniel Mitchell, Jamie Blanche, Sam Harper, Wenshuo Tang, Ketan Pancholi, Lee Baines, David G Bucknall, David Flynn, A review of sensing technologies for non-destructive evaluation of structural composite materials, J. Compos. Sci. 5 (2021).

[6] K.P. Desai, D. Binu, A.V.V.D. Pavan, A.P. Kamath, Automation advancements in wind turbine blade production: A review, in: Lecture Notes in Mechanical Engineering, Springer Science and Business Media Deutschland GmbH, 2022, pp. 209–222.

[7] Engaging Autopilot: NREL Explores Automation To Build Better Blades, Lower Costs, and Transform Wind Technology Manufacturing | News | NREL.

[8] Helena Solman, Julia Kirch Kirkegaard, Mattijs Smits, Bas Van Vliet, Simon Bush, Digital twinning as an act of governance in the wind energy sector, Environ. Sci. Policy 127 (2022) 272–279.

[9] Mengnan Liu, Shuiliang Fang, Huiyue Dong, Cunzhi Xu, Review of digital twin about concepts, technologies, and industrial applications, J. Manuf. Syst. 58 (2021) 346–361, Digital Twin towards Smart Manufacturing and Industry 4.0.

[10] Reinforced Plastics, Digital wind blade manufacture, 2023.

[11] Xiao Chen, Martin A. Eder, A.S.M. Shihavuddin, Dan Zheng, A human-cyber-physical system toward intelligent wind turbine operation and maintenance, Sustainability 13 (2021) 561.

[12] J. Blanche, D. Mitchell, R. Gupta, A. Tang, D. Flynn, Asset integrity monitoring of wind turbine blades with non-destructive radar sensing, in: 2020 11th IEEE Annual Information Technology, Electronics and Mobile Communication Conference, IEMCON, 2020, pp. 498–504.

[13] Hossein Montazerian, Armin Rashidi, Abbas S. Milani, Mina Hoorfar, Integrated sensors in advanced composites: A critical review, (ISSN: 15476561) 2019, 45: 187–238. http://dx.doi.org/10.1080/10408436.2019.1588705.

[14] Sahar Hassani, Mohsen Mousavi, Amir H. Gandomi, Structural health monitoring in composite structures: A comprehensive review, Sensors 22 (2021) 153.

[15] Jamie Blanche, Daniel Mitchell, David Flynn, Run-time analysis of road surface conditions using non-contact microwave sensing, 2020.

[16] D. Mitchell, J. Blanche, D. Flynn, An evaluation of millimeter-wave radar sensing for civil infrastructure, in: 2020 11th IEEE Annual Information Technology, Electronics and Mobile Communication Conference, IEMCON, 2020, pp. 216–222.

[17] Wenshuo Tang, Daniel Mitchell, Jamie Blanche, Ranjeetkumar Gupta, David Flynn, Machine learning analysis of non-destructive evaluation data from radar inspection of wind turbine blades, in: 2021 IEEE International Conference on Sensing, Diagnostics, Prognostics, and Control, SDPC, 2021, pp. 122–128.

[18] Wenshuo Tang, Jamie Blanche, Daniel Mitchell, Samuel Harper, David Flynn, Characterisation of composite materials for wind turbines using frequency modulated continuous wave sensing, J. Compos. Sci. 7 (2023) 75.

[19] J Blanche, H Lewis, G Couples, J Buckman, N Lenoir, A Tengattini, D Flynn, Dynamic fluid ingress detection in geomaterials using K-band frequency modulated continuous wave radar, IEEE Access (2020).

[20] Jamie Blanche, Jim Buckman, Helen Lewis, David Flynn, Gary Couples, Frequency modulated continuous wave analysis of dynamic load deformation in geomaterials, in: Offshore Technology Conference, Society of Petroleum Engineers (SPE), Houston, Tx, 2020.

[21] Mohammad Jawaid, Mohamed Thariq, Advanced composite materials for aerospace engineering : processing, properties and applications.

[22] Dongliang Wang, Binbin Liao, Jinyang Zheng, Gai Huang, Zhengli Hua, Chaohua Gu, Ping Xu, Development of regulations, codes and standards on composite tanks for on-board gaseous hydrogen storage, Int. J. Hydrogen Energy 44 (2019) 22643–22653.

[23] Hai Fang, Yu Bai, Weiqing Liu, Yujun Qi, Jun Wang, Connections and structural applications of fibre reinforced polymer composites for civil infrastructure in aggressive environments, Composites B 164 (2019) 129–143.

[24] David M.J. Tax, Robert P.W. Duin, Support vector data description, Mach. Learn. 54 (2004) 45–66.

[25] Yuna Pan, Daolai Cheng, Tingting Wei, Yuchen Jia, Rolling bearing performance degradation assessment based on deep belief network and improved support vector data description, Mech. Syst. Signal Process. 181 (2022) 109458.

[26] Zhi Tang, Xiaofeng Liu, Daiping Wei, Honglin Luo, Pu Jiang, Lin Bo, Enhanced multiclass support vector data description model for fault diagnosis of gears, Measurement 194 (2022) 110974.

[27] Yuxuan Zhang, Xiaoyou Wang, Zhenghao Ding, Yao Du, Yong Xia, Anomaly detection of sensor faults and extreme events based on support vector data description, Struct. Control Health Monit. 29 (10) (2022) e3047.

[28] Lukas Ruff, Robert A Vandermeulen, Nico Görnitz, Alexander Binder, Emmanuel Müller, Klaus-Robert Müller, Marius Kloft, Deep semi-supervised anomaly detection, 2019, arXiv preprint arXiv:1906.02694.

[29] Ehtesamul Azim, Dongjie Wang, Yanjie Fu, Deep graph stream SVDD: Anomaly detection in cyber-physical systems, 2023, arXiv preprint arXiv:2302.12918.

[30] Songqiao Han, Xiyang Hu, Hailiang Huang, Mingqi Jiang, Yue Zhao, Adbench: Anomaly detection benchmark, 2022, arXiv preprint arXiv:2206.09426.

[31] Joshua Bassey, Lijun Qian, Xianfang Li, A survey of complex-valued neural networks, 2021, arXiv preprint arXiv:2101.12249.

[32] Matthew Russell, Peng Wang, Physics-informed deep learning for signal compression and reconstruction of big data in industrial condition monitoring, Mech. Syst. Signal Process. 168 (2022) 108709.

[33] Sindy Löwe, Phillip Lippe, Maja Rudolph, Max Welling, Complex-valued autoencoders for object discovery, 2022, arXiv preprint arXiv:2204.02075.

[34] Mhd Modar Halimeh, Walter Kellermann, Complex-valued spatial autoencoders for multichannel speech enhancement, in: ICASSP 2022-2022 IEEE International Conference on Acoustics, Speech and Signal Processing, ICASSP, IEEE, 2022, pp. 261–265.

[35] Lukas Piotrowsky, Vladimir Bernhardt, Jan Barowski, Ilona Rolfes, Nils Pohl, Antenna pattern characterization with an industrial robot assisted fmcw radar system, in: 2019 IEEE Asia-Pacific Microwave Conference, APMC, IEEE, 2019, pp. 153–155.

[36] Huan He, Owen Queen, Teddy Koker, Consuelo Cuevas, Theodoros Tsiligkaridis, Marinka Zitnik, Domain adaptation for time series under feature and label shifts, 2023, arXiv preprint arXiv:2302.03133.

[37] Douw Gerbrand Marx, Chenyu Liu, Jerome Antoni, Konstantinos Gryllias, Deep learning implementations of cyclo-stationary signal processing methods, in: 2022 Leuven Conference on Noise and Vibration Engineering, 2022.

[38] Kota Dohi, Tomoya Nishida, Harsh Purohit, Ryo Tanabe, Takashi Endo, Masaaki Yamamoto, Yuki Nikaido, Yohei Kawaguchi, MIMII DG: Sound dataset for malfunctioning industrial machine investigation and inspection for domain generalization task, 2022, arXiv preprint arXiv:2205.13879.

[39] Manuel Arias Chao, Bryan T. Adey, Olga Fink, Implicit supervision for fault detection and segmentation of emerging fault types with deep variational autoencoders, Neurocomputing 454 (2021) 324–338.

[40] Viet-Tuan Le, Yong-Guk Kim, Attention-based residual autoencoder for video anomaly detection, Appl. Intell. 53 (3) (2023) 3240–3254.

[41] Hyunseong Lee, Hyung Jin Lim, Travis Skinner, Aditi Chattopadhyay, Asha Hall, Automated fatigue damage detection and classification technique for composite structures using lamb waves and deep autoencoder, Mech. Syst. Signal Process. 163 (2022) 108148.

[42] Lukas Ruff, Robert Vandermeulen, Nico Goernitz, Lucas Deecke, Shoaib Ahmed Siddiqui, Alexander Binder, Emmanuel Müller, Marius Kloft, Deep one-class classification, in: International Conference on Machine Learning, PMLR, 2018, pp. 4393–4402.

[43] Xavier Glorot, Antoine Bordes, Yoshua Bengio, Deep sparse rectifier neural networks, in: Proceedings of the Fourteenth International Conference on Artificial Intelligence and Statistics, JMLR Workshop and Conference Proceedings, 2011, pp. 315–323.

[44] Martin Arjovsky, Amar Shah, Yoshua Bengio, Unitary evolution recurrent neural networks, in: International Conference on Machine Learning, PMLR, 2016, pp. 1120–1128.

[45] Chiheb Trabelsi, Olexa Bilaniuk, Ying Zhang, Dmitriy Serdyuk, Sandeep Subramanian, Joao Felipe Santos, Soroush Mehri, Negar Rostamzadeh, Yoshua Bengio, Christopher J Pal, Deep complex networks, 2017, arXiv preprint arXiv:1705.09792.

[46] Laurens Van der Maaten, Geoffrey Hinton, Visualizing data using t-SNE, J. Mach. Learn. Res. 9 (11) (2008).

[47] Sridhar Ramaswamy, Rajeev Rastogi, Kyuseok Shim, Efficient algorithms for mining outliers from large data sets, in: Proceedings of the 2000 ACM SIGMOD International Conference on Management of Data, 2000, pp. 427–438.

[48] Fei Tony Liu, Kai Ming Ting, Zhi-Hua Zhou, Isolation forest, in: 2008 Eighth IEEE International Conference on Data Mining, IEEE, 2008, pp. 413–422.

[49] Markus M Breunig, Hans-Peter Kriegel, Raymond T Ng, Jörg Sander, LOF: identifying density-based local outliers, in: Proceedings of the 2000 ACM SIGMOD International Conference on Management of Data, 2000, pp. 93–104.

[50] Jinwon An, Sungzoon Cho, Variational autoencoder based anomaly detection using reconstruction probability, Special Lect. IE 2 (1) (2015) 1–18.

[51] Yue Zhao, Zain Nasrullah, Zheng Li, Pyod: A python toolbox for scalable outlier detection, 2019, arXiv preprint arXiv:1901.01588.